

# Anisotropic imbibition on surfaces patterned with polygonal posts

MATTHEW L. BLOW\* † and JULIA M. YEOMANS

*The Rudolf Peierls Centre for Theoretical Physics, Oxford University, 1 Keble Road, Oxford OX1 3NP, England*

We present and interpret lattice Boltzmann simulations of thick films spreading on surfaces patterned with polygonal posts. We show that the mechanism of pinning and depinning differs with the direction of advance, and demonstrate that this leads to anisotropic spreading within a certain range of material contact angles.

## I. INTRODUCTION

A drop placed on a partially wetting substrate will make a finite angle with the surface, given by Young's equation [1],

$$\cos \theta_Y = \frac{\gamma_{SV} - \gamma_{SL}}{\gamma}, \quad (1)$$

where  $\gamma_{SV}$ ,  $\gamma_{SL}$  and  $\gamma$  are the solid–vapour, solid–liquid and liquid–vapour surface tensions. Young's equation assumes that the surface is smooth, and that the contact line is able to move freely to allow the drop to globally minimise its free energy.

Due to recent advances in microlithography it is now possible to pattern surfaces with regular arrays of micron-scale posts, leading to deviations from Young's equation on a macroscopic level. On a superhydrophilic, or superwetting surface, the fluid can be drawn into the spaces between the posts, such that the drop forms a film with thickness equal to the height of the posts [2–4], a phenomenon that is termed imbibition.

Imbibition is thermodynamically feasible if the thick film has a lower free energy than the dry surface. The free energy change per unit width,  $\delta\mathcal{F}$ , when the film advances a distance  $\delta x$  can be estimated by averaging over the surface features

$$\delta\mathcal{F} = [(\gamma_{SL} - \gamma_{SV})(r - \phi) + \gamma(1 - \phi)] \delta x, \quad (2)$$

where  $r$  is the ratio of the surface area to its vertical projection,  $\phi$  is the fraction of the surface covered by posts, and we assume posts of constant cross-section. Eliminating the surface tensions in Eqn. (2) using Eqn. (1), the condition  $\delta\mathcal{F} < 0$  becomes [2]

$$\cos \theta_Y > \cos \theta_I = \frac{1 - \phi}{r - \phi}. \quad (3)$$

This inequality relies on the same assumption as Young's equation (1): namely that the contact line can move freely over the substrate, sampling the average properties of the roughness. This assumption holds well on some surfaces, for example, in the longitudinal direction on a grooved surface, but not in other cases, for example perpendicular to such grooves, where free energy barriers due to contact line pinning can halt the motion of the interface [5].

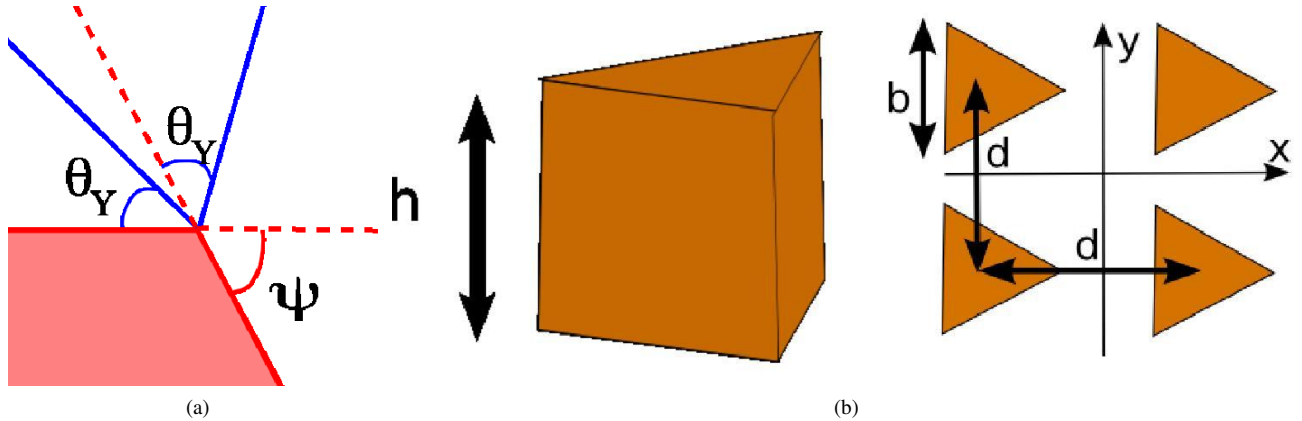


FIG. 1: (a) Illustration of the Gibbs' Criterion. At a sharp corner a wetting contact line remains pinned for all angles between  $\theta_Y$  and  $\theta_Y + \psi$  (between the full lines). (b) Diagram showing the geometry and post dimensions for the simulations described in Sec. III.

\* Now at: Centro de Física Teórica e Computacional (CFTC), University of Lisbon, Instituto de Investigação Interdisciplinar, Av. Prof. Gama Pinto, 2, Lisboa, 1649-003, Portugal

† email: matthewblow@gmail.com

Contact line pinning occurs when an interface moving across a surface meets a convex corner. The criterion for pinning, proposed by Gibbs [6] and demonstrated experimentally by Oliver *et al.* [7], is that the contact angle can take a range of values spanning the dihedral angle of the corner, as shown in Fig. 1(a). Over this range, the contact angle with respect to the dry plane is too low for the contact line to advance, and that with the wet plane is too high for the contact line to recede. Pinning on surface features can lead to the threshold angle for imbibition being substantially lower than prediction (3), as was demonstrated by Courbin *et al* [8, 9]. Furthermore it has been shown that anisotropic surface features lead to anisotropic spreading [10, 11]. In these proceedings, we use the lattice Boltzmann method to study imbibition through an array of posts with uniform polygonal cross-section, building on previous work [12]. We show that the mechanism of contact line pinning differs with direction, and explain how this leads to anisotropic spreading.

## II. SIMULATION APPROACH

We model the system as a diffuse-interface, two-phase fluid in contact with a solid substrate. The thermodynamic state of the fluid is described by an order parameter  $\rho(\mathbf{r})$ , corresponding to the density of the fluid at each point  $\mathbf{r}$ . The equilibrium properties are modelled by a Landau free energy functional over the spatial domain of the fluid  $\mathcal{D}$ , and its boundary with solid surfaces  $\partial\mathcal{D}$ ,

$$\Psi = \iiint_{\mathcal{D}} (p_c \{ \nu^4 - 2\beta\tau_w(1 - \nu^2) - 1 \} - \mu_b\rho + \frac{1}{2}\kappa|\nabla\rho|^2) dV - \iint_{\partial\mathcal{D}} \mu_s\rho dS. \quad (4)$$

The first term in the integrand of (4) is the bulk free energy density, where  $\nu = (\rho - \rho_c)/\rho_c$  and  $\rho_c$ ,  $p_c$ , and  $\beta\tau_w$  are constants. It allows two equilibrium bulk phases, liquid and gas, with  $\nu = \pm\sqrt{\beta\tau_w}$ . The second term is a Lagrange multiplier constraining the total mass of the fluid. The third term is a free energy cost associated with density gradients. This allows for a finite-width, or diffuse, interface to arise between the bulk phases, with surface tension  $\gamma = \frac{4}{3}\rho_c\sqrt{2\kappa p_c(\beta\tau_w)^3}$  and width  $\chi = \frac{1}{2}\rho_c\sqrt{\kappa/(\beta\tau_w p_c)}$ . The boundary integral takes the form proposed by Cahn [13]. Minimising the free energy leads to a Neumann condition on the density

$$\partial_{\perp}\rho = -\mu_s/\kappa. \quad (5)$$

The wetting potential  $\mu_s$  related to the  $\theta_Y$  of the substrate by [17]

$$\mu_s = 2\beta\tau_w\sqrt{2p_c\kappa}\text{sign}\left(\frac{\pi}{2} - \theta_Y\right)\sqrt{\cos\frac{\alpha}{3}\left(1 - \cos\frac{\alpha}{3}\right)}, \quad \alpha = \arccos(\sin^2\theta_Y). \quad (6)$$

The hydrodynamics of the fluid is described by the continuity and the Navier-Stokes equations

$$\partial_t\rho + \partial_{\alpha}(\rho u_{\alpha}) = 0, \quad (7)$$

$$\partial_t(\rho u_{\alpha}) + \partial_{\beta}(\rho u_{\alpha}u_{\beta}) = -\partial_{\beta}P_{\alpha\beta} + \partial_{\beta}(\rho\eta\{\partial_{\beta}u_{\alpha} + \partial_{\alpha}u_{\beta}\} + \rho\lambda\delta_{\alpha\beta}\partial_{\gamma}u_{\gamma}), \quad (8)$$

where  $\mathbf{u}$  is the local velocity,  $\mathbf{P}$  is the pressure tensor derived from the free energy functional (4) and  $\eta$  and  $\lambda$  are the shear and bulk kinematic viscosities respectively. A free energy lattice Boltzmann algorithm is used to numerically solve Eqns. (7,8) [14–16]. At the substrate we impose the boundary condition (5) [17, 18], and a condition of no-slip [19–21].

We choose  $\kappa = 0.01$ ,  $p_c = 0.125$ ,  $\rho_c = 3.5$ ,  $\tau_w = 0.3$  and  $\beta = 1.0$ , giving an interfacial thickness  $\chi = 0.9$ , surface tension  $\gamma = 0.029$  and a density ratio of 3.42. The viscosity ratio is  $\eta_L/\eta_G = 7.5$ .

## III. IDENTIFYING THE PINNING MECHANISMS

We consider a rectangular array of posts on a flat substrate. The cross-section of each post is uniform, and is an equilateral triangle, oriented to point along a primary axis of the array taken to be the  $x$ -direction (see Fig. 1(b)). In our simulations we hold the array spacing  $d$  and post side-length  $b$  at 40 and 20 lattice units respectively and vary the post height  $h$ . We find that rescaling the system such that  $d = 60$  does not change the threshold angles of spreading significantly[23]. The posts and substrate are taken to have the same Young angle  $\theta_Y$ .

We consider the advance of a straight contact line, which is parallel to the  $y$ -axis. We exploit periodic boundary conditions and use a simulation box of length  $d_y$  along  $y$ . We further halve the computational burden by taking  $x = 0$  as a plane of reflectional symmetry, and we compare the dynamics for triangles pointing away from, or towards, the origin. To simulate imbibition fed by a mother drop resting on the surface would require a very large simulation box, and be prohibitively costly in terms of computer time. Since we are only interested in the details of flow amongst the posts, we instead feed imbibition from a ‘virtual reservoir’, a small region  $\sim 6$  lattice points wide spanning the centre of the box where  $\nu$  is fixed to  $\sqrt{\beta\tau_w}$  at each time step of the simulation.

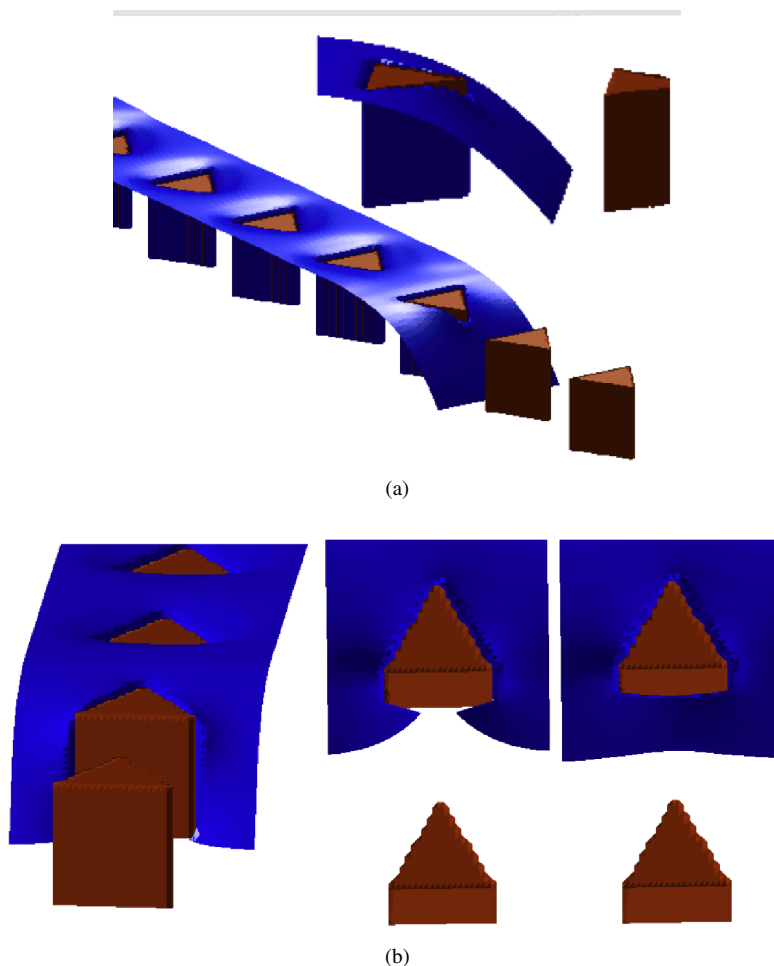


FIG. 2: Snapshots of (a) the *connected contact line* and (b) the *disconnected contact line* mechanisms of pinning. In the middle image of (b) a gap appears between the interface and the face of the post. This is because the liquid (blue) surface represents the density  $\rho_c$ , and close to the concave corner the wetting potential increases the density above  $\rho_c$

In this way, liquid is introduced while there is outwards flow, but once the interface is fully pinned, no new liquid enters the system.

$\theta_Y$  is then decreased quasistatically, and we record the value at which depinning and spreading to the next post occurs. For the geometry we describe, Eqn. (3), which describes imbibition with no pinning, gives an upper bound of the threshold angle of [2]

$$\sec \theta_I = 1 + \frac{12bh}{4d^2 - \sqrt{3}b^2} = 1 + \frac{12h/b}{16 - \sqrt{3}}. \quad (9)$$

#### A. Pinning of a connected interface

Snapshots showing one pinning mechanism, for a film advancing in the direction of the points of the triangles, are shown in Fig. 2(a). The film is of height  $h$  up to the leading triangle, and then descends with increasing  $x$  to meet the substrate at the Young angle. There are two ways in which the contact line can move forward. Firstly, it could make a shallower angle at the substrate, but this would increase the free energy away from the minimum characterised by Eqn. (1). Secondly, the top of the film could move forwards, but this would create liquid-gas interface and hence also have a free energy cost.

Depinning will occur when  $\theta_Y$  is sufficiently small that the contact line on the base reaches the next post. This depinning pathway, which we shall term the *connected contact line* mechanism, was elucidated by Courbin et al[8, 9], who showed that

$$\tan \theta_I = \frac{\text{post height}}{\text{post spacing}} = \frac{h}{d - \frac{\sqrt{3}}{2}b} = \frac{h/b}{2 - \frac{\sqrt{3}}{2}}. \quad (10)$$

Numerical results for the variation of the depinning angle with  $h/b$  are shown in Fig. 3 as indigo circles, and Eqns. (9, 10) are

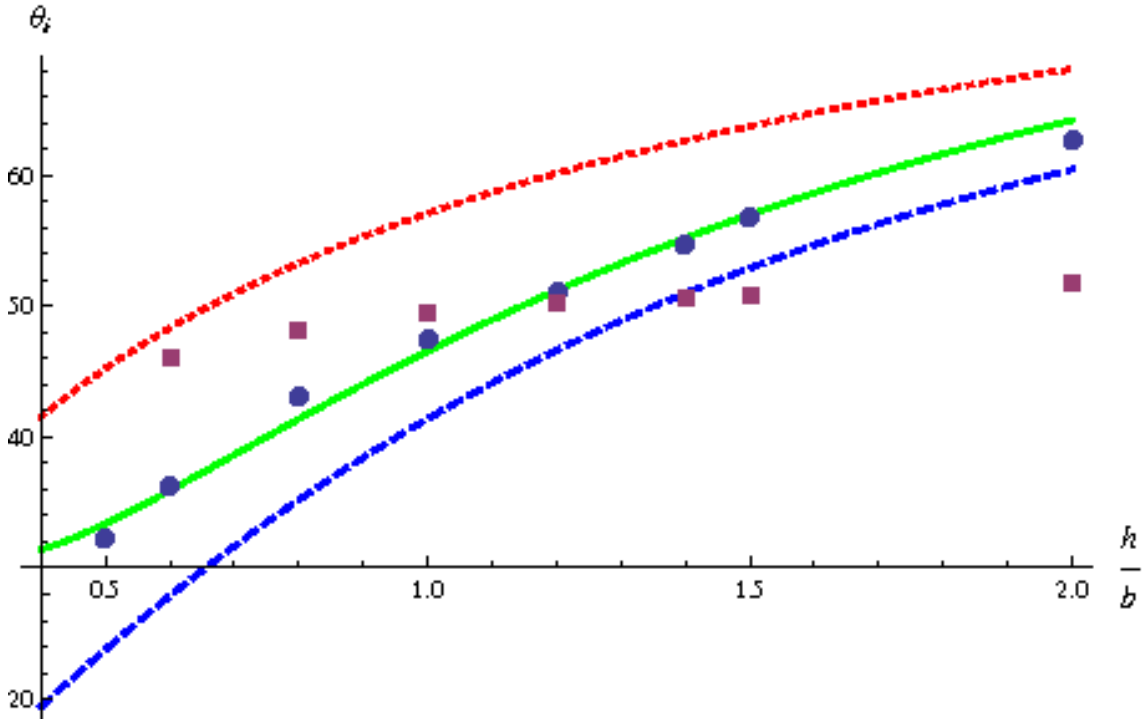


FIG. 3: The threshold angle for depinning along  $+x$  (indigo circles) and  $-x$  (mauve squares) as a function of  $h/b$ . Depinning in these directions occurs according to the connected and disconnected contact line mechanisms respectively. The predictions from Eqns. (9) in red (dotted), (10) in blue (dashed), and (12) in green (full) are plotted for comparison.

plotted as red and blue curves respectively. Comparing the simulation data to the blue curve, we see that the simulation values are significantly higher than those predicted, especially for lower values of  $h/b$ .

To resolve the discrepancy we note that Eqn. (10) assumes a flat interface. A positive Laplace pressure  $\Delta p$  will instead produce a convex curvature, enabling the interface to extend further across the substrate. Neglecting curvature in the  $y$  direction, we model the interface in the  $xz$  plane as a circular arc with radius of curvature  $R = \gamma/\Delta p$  given by Laplace's law. The contact angle with the substrate will then be modified to

$$\tan(\theta_1 - \beta) = \frac{h}{s}, \quad (11)$$

where  $\beta$  is the angle of bulge, given by  $\sqrt{h^2 + s^2} = 2R \sin \beta$ . The depinning threshold is thus given by

$$\theta_1 = \arctan\left[\frac{h}{s}\right] + \arcsin\left[\frac{\sqrt{h^2 + s^2}}{2R}\right]. \quad (12)$$

We expect the dominant contribution to the Laplace pressure to result from confinement in the  $z$  direction. Therefore, we shall assume  $\Delta p \propto h^{-1}$ . Writing  $R = Ah$  and  $s = d - Bb$ , a least squares fit of the data to Eqn. (12), with respect to  $A$  and  $B$ , was performed. The optimisation found  $B = 0.822$ , barely different from the value  $\frac{\sqrt{3}}{2} \approx 0.866$  used in Eqn. (9), and  $A = 7.09$ . Eqn. (12) is plotted with these coefficients as the green curve in Fig. 3, and the fit is very reasonable.

### B. Pinning of a disconnected interface

We now present simulation results with the posts pointing towards the origin, and identify a second mechanism for (de)pinning, shown in Fig. 2(b). Now the advancing front is disconnected, and is pinned at the vertical edges of the posts. The base of the film is pulled forward by the hydrophilic substrate, but there is a free energy cost associated with the growth of the interface as it spreads out from the gap. As the Young angle is quasistatically decreased, the contact line creeps onto the blunt faces of the posts, near to the base substrate, but remains pinned to the post edges at higher  $z$ , where the angle made between the interface and the blunt faces remains less than  $\theta_Y$ . When  $\theta_Y$  becomes sufficiently small, the depinned parts of the contact lines from neighbouring gaps meet each other midway. Once connected, the interface readily wets up the posts and out across the substrate.

We shall refer to this as the *disconnected contact line* pinning mechanism. The threshold for depinning is plotted in Fig. 3 as mauve squares. The dependence on  $h/b$  is different to that for motion along  $+x$ . When  $h/b$  is low, the depinning angle closely follows the upper bound given by Eqn. (9), indicating that pinning by the posts is weak in this regime. For larger values of the ratio  $h/b$ ,  $\theta_1$  levels off to  $\sim 51^\circ$ .

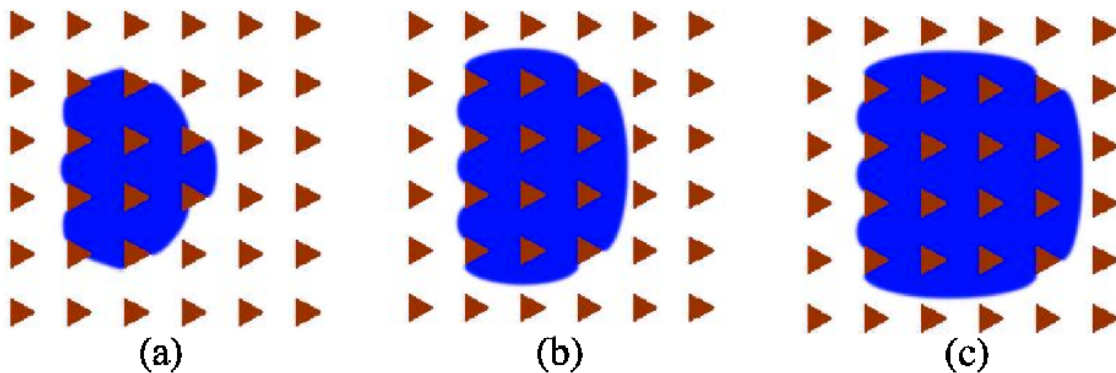
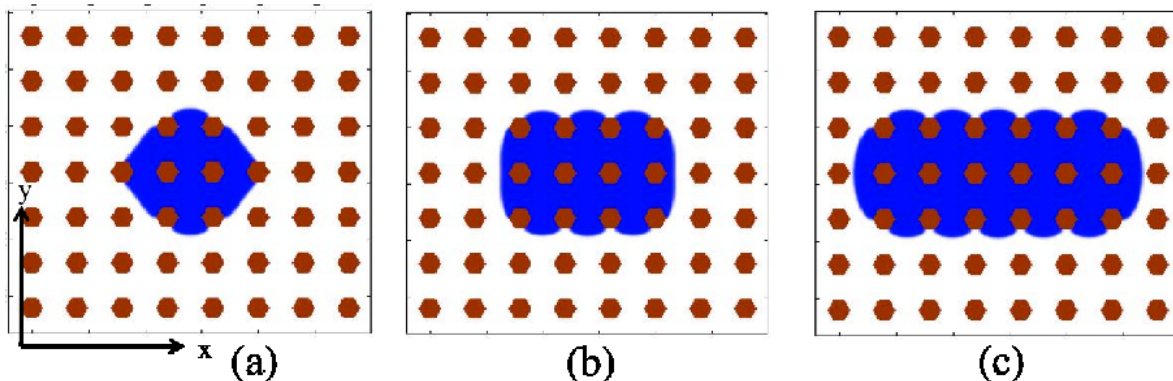


FIG. 4: Spreading on a square array of triangles

FIG. 5: Hexagonal posts show the connected contact line mechanism along  $\pm x$  and the disconnected contact line mechanism along  $\pm y$ .

#### IV. IMBIBITION THROUGH POLYGONAL POSTS

We now present simulation results for films spreading through arrays with various lattice symmetries and post geometries. We use arrays which are several posts wide in both the  $x$  and  $y$  directions, such that the film is not connected over periodic boundaries. We again use a virtual reservoir, this time located at a small location at the centre of the array, but we hold  $\theta_Y$  constant over time. We discern how both the arrangement, and the geometries, of the posts affect the dynamics of the interfaces, and the final film shapes. These can be interpreted in terms of the pinning mechanisms identified in Sec. III.

For our simulations we use  $d = 40$ ,  $b = 20$ ,  $h = 30$  and  $\theta_Y = 55^\circ$ . According to Fig. 3, these parameters should allow and inhibit spreading in the  $+x$  and  $-x$  directions respectively. In Figs. 4, 5 and 6, we show plan views of the substrate at various times in the evolution of the film. The posts are shown in brown, the wetted substrate in blue, and the unwetted substrate in white.

##### A. A square array of triangular posts

We first consider the system studied in Sec. III, extended in the  $y$  direction. The shape of the film at intermitant times is shown in Fig. 4. Advance of the film is possible in the  $+x$  and  $\pm y$  directions, via the connected contact line mechanism, but the film is barred from advancing in the  $-x$  direction, where the disconnected contact line mechanism, which has a lower threshold angle, is relevant. Thus the surface acts as a microfluidic diode. Such unidirectional behaviour is made possible by the triangular shape of the posts.

##### B. A square array of hexagonal posts

Having considered exclusively triangular posts thus far in the chapter, we now turn our attention to posts whose cross-sections are regular hexagons. We find that the two depinning mechanisms discerned for triangles, in Sec. III, may also be applied to hexagons, but that their directional distribution of occurrence is different. We consider hexagonal posts in a square array, oriented so that the corners point along  $\pm x$ . Along these two directions, as might be expected, the (de)pinning behaviour follows the

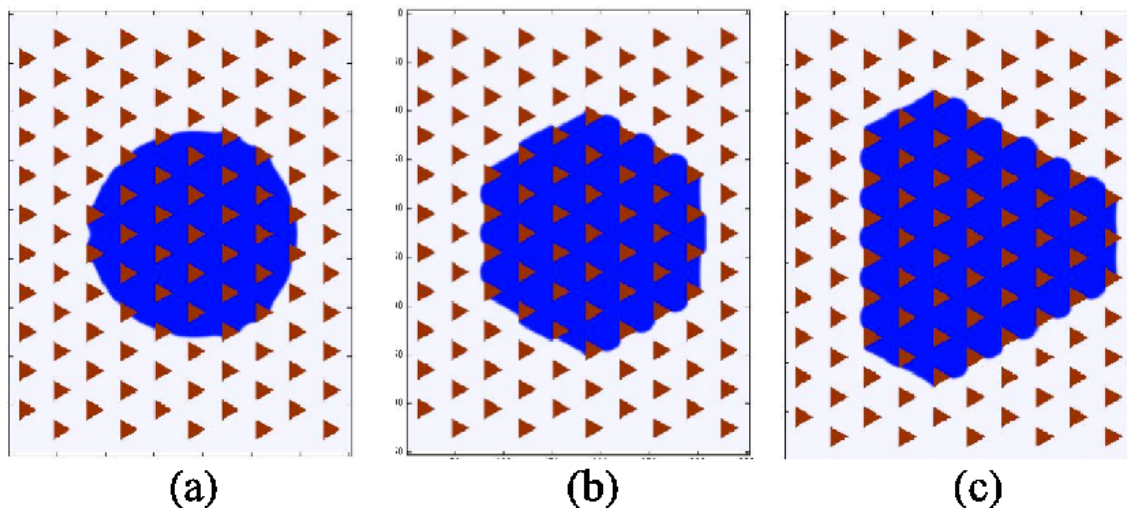


FIG. 6: Spreading on a hexagonal array of triangles

connected contact line mechanism. Conversely, the faces point along  $\pm y$ , and it is the disconnected contact line mechanism which determines the (de)pinning in these directions. Fig. 5 shows the spreading of a film on a square array of hexagons. Since advance of the liquid is permitted along  $\pm x$  but barred along  $\pm y$ , a stripe of fluid is formed.

### C. A hexagonal array of triangular posts

We now simulate a hexagonal lattice of posts with spacing  $d = 40$ , and the triangles aligned with lattice directions, as shown in Fig. 6. We start with a circular film with diameter spanning several posts (Fig. 6(a)). As spreading begins, the film quickly facets into a hexagon, by aligning its sides with posts in the immediate vicinity (Fig. 6(b)). Spreading continues, via the connected contact line mechanism, along the directions of the three corners of the posts, but the interface is pinned, by the disconnected contact line mechanism, along the faces. As a result, the facets along the corner directions shrink as they advance (Fig. 6(c)).

## V. DISCUSSION

We have performed Lattice Boltzmann simulations of imbibition on hydrophilic substrates patterned with posts, whose cross-sections are regular polygons. Our motivation was to identify pinning mechanisms on the posts and show how these lead to anisotropic spreading behaviour on the surface.

We began by considering the advance of a long planar front along a row of triangular posts. This enabled us to take advantage of periodic boundaries in the simulations, reducing computational expense, and to isolate particular pinning behaviours. The simulations showed that the critical value of  $\theta_Y$  at which the interface advances differs between directions relative to the triangles. Hence there is a range of  $\theta_Y$  in which spreading is unidirectional, with the exact range and direction of the anisotropy depending on the relative dimensions of the substrate. The cause is differing depinning routes: one where the contact line along the base substrate is connected, and one where it is disconnected, punctuated by the blunt edges of the posts.

We showed that a square lattice of triangular posts inhibits spreading in one direction, while if hexagonal posts are used, the spreading is bidirectional, with films elongating. Finally we investigated spreading amongst a hexagonal lattice of triangular posts. The three-fold rotational symmetry of this geometry leads to the formation of a triangular film.

In future work it would be of interest to consider how the spreading is affected if the post cross section changes with height, and how electrowetting might be used to locally control the contact angle, and hence the spreading characteristics [22].

### Acknowledgments

We thank H. Kusumaatmaja, B. M. Mognetti and R. Vrancken for helpful discussions.

- 
- [1] T. Young, *Philos. Trans. R. Soc. London* **95**, (1805) 65
  - [2] J. Bico, C. Tordeux and D. Quéré, *Europhys. Lett.* **55**, (2001) 214
  - [3] C. Ishino, M. Reyssat, E. Reyssat, K. Okumura and D. Quéré, *Europhys. Lett.* **79**, (2007) 56005
  - [4] C. Ishino and K. Okumura, *Europhys. J. E* **25**, (2008) 415
  - [5] Y. Chen, B. He, J. Lee and N. J. Patankar, *J. Colloid Interface Sci.* **281** (2005), 458
  - [6] J. W. Gibbs *The Scientific Papers of J. Willard Gibbs* Dover Publications, New York (1961)
  - [7] J. F. Oliver, C. Huh and S. G. Mason, *J. Colloid Interface Sci.* **59**, (1977) 568
  - [8] L. Courbin, E. Denieul, E. Dressaire, M. Roper, A. Adjari and H. A. Stone, *Nat. Mat.* **6**, (2007) 661
  - [9] L. Courbin, J. C. Bird, M. Reyssat, and H. A. Stone, *J. Phys. Cond. Mat.* **21**, (2009) 46
  - [10] T. I. Kim and K. Y. Suh, *Soft Matter* **5**, (2009) 4131
  - [11] K. H. Chu, R. Xiao and E. N. Wang, *Nat. Mat.* **9**, (2010) 413
  - [12] M. L. Blow, H. Kusumaatmaja and J. M. Yeomans *J. Phys.: Condens. Matter* **21**, (2009) 464125
  - [13] J. W. Cahn *J. Chem. Phys.* **66**, (1977) 3667
  - [14] M. R. Swift, E. Orlandini, W. R. Osborn and J. M. Yeomans, *Phys. Rev. E* **54**, (1996) 5041
  - [15] S. Succi *The Lattice Boltzmann Equation for Fluid Dynamics and Beyond*, Oxford Univ. Press, Oxford (2001)
  - [16] J. M. Yeomans *Physica A* **369**, (1996) 159
  - [17] A. J. Briant, A. J. Wagner and J. M. Yeomans, *Phys. Rev. E* **69**, (2004) 031602
  - [18] A. Dupuis and J. M. Yeomans, *Langmuir* **21**, (2005) 2624
  - [19] A. J. C. Ladd, *J. Fluid. Mech.* **271**, (1994) 285
  - [20] C. M. Pooley, H. Kusumaatmaja and J. M. Yeomans, *European Physical Journal Special Topics* **171** (2009) 63
  - [21] M. Bouzidi, M. Firdaouss and P. Lallemand, *Phys. Fluids* **13**, (2001) 1070
  - [22] M. Dhindsa, J. Heikenfeld, S. Kwon, J. Park, P. D. Rack and I. Papautsky *Lab Chip* **10** (2009), 801
  - [23] Reducing the system size to  $d = 20$  leads to slightly lower values for the depinning thresholds which explains the small quantitative differences to the results we present in [12]